CRISPR-NSID: an *in vivo* CRISPR/Cas9 negative selection screen reveals EZH2 as a druggable dependency factor in a genetic desmoid tumor model.

Thomas Naert[1,2], Tom Van Nieuwenhuysen[1,2], Suzan Demuynck[1,2], Sven de Grande[1], Joanna Przybyl[3], Marnik Vuylsteke[4], Rivka Noelanders[1], Dieter Tulkens[1,2], Dionysia Dimitrakopoulou[1,2], David Creytens[2,5], Matt van de Rijn[3], Savvas Savvides[6,7] and Kris Vleminckx[1,2,8]

[1] Department of Biomedical Molecular Biology, Ghent University, Ghent, Belgium

[2] Cancer Research Institute Ghent, Ghent, Belgium

[3] Department of Pathology, Stanford University School of Medicine, Stanford, USA

[4] GNOMIXX ltd, Statistics for Genomics, Melle, Belgium

[5] Department of Pathology, Ghent University and Ghent University Hospital, Ghent, Belgium

[6] Unit for Structural Biology, Department of Biochemistry and Microbiology, Ghent University, Technologiepark 71, 9052, Zwijnaarde (Ghent), Belgium.

[7] Unit for Structural Biology, VIB Center for Inflammation Research, Technologiepark 71, 9052, Zwijnaarde, (Ghent), Belgium.

[8] Center for Medical Genetics, Ghent University, Ghent, Belgium

Abstract

Identification of true dependencies in cancer is pivotal to the elucidation of novel therapeutic strategies to increase prospects for cancer patients. Unfortunately, *in vivo* identification of genetic dependencies has long relied on expensive and time-consuming breeding of genetically engineered animal models. Recently, *in vitro* CRISPR/Cas9 screens provided a new method for rapid and genome-wide identification of genetic dependencies. Nevertheless, genetic dependencies would ideally be identified using *in vivo* cancer models initiated by clinically relevant oncogenic driver or tumor suppressor insults. Here, we report a new methodology called **CRISPR**/Cas9-mediated **N**egative **S**election **I**dentification of genetic **D**ependencies (**CRISPR-NSID**) that allows *in vivo* elucidation of cancer cell vulnerabilities in genetic cancer models. The methodology hinges on the fact that for a genetic dependency there is an incapability for recovering tumors carrying biallelic frameshift mutations in this gene. We demonstrate how integrating experimentally determined, or *in silico* predicted, probabilities of frameshift editing for any given gRNA can be employed to ascertain negative selection pressure on inactivation of a genetic dependency during tumorigenesis. As a proof-of-principle, we use CRISPR-NSID to identify *ezh2* and *creb3l1* as genetic dependencies in desmoid tumors (desmoid-type fibromatosis) occurring in a *Xenopus tropicalis* cancer model driven by *apc* mutations. Bridging CRISPR-NSID to a clinically unmet need, we further demonstrate the promise for EZH2 inhibition as a new therapeutic strategy for desmoid tumors. This study establishes a new methodology for rapid identification of genetic dependencies in monoclonal disorders with wide adaptability to other model systems and organisms.

Introduction

Genome-scale viability-based negative selection screens using CRISPR/Cas9 have emerged as a powerful technique for identification of cancer cell vulnerabilities[1–3]. *In vivo* and smaller scale negative selection screens have also been described, employing CRISPR/Cas9 libraries transduced in cancer cell cultures subsequently transferred into sub-lethally irradiated mice[4]. However and ideally, genuine *in vivo* negative selection screens should take place in autochthonous tumors that are preferentially induced by genetic modification of clinically relevant cancer drivers[5]. While previously published work has hinted at the possibility of *in vivo* CRISPR/Cas9-based negative selection identification of genetic dependencies[6], to our knowledge, the methodology and a proof-of-principle have not been previously reported. In negative-selection CRISPR screens, the feasibility of Cas9 to generate in-frame insertions-deletions (INDELs) has previously been considered a nuisance, as these in-frame mutations can encode protein with intact functions, allowing escape of imposed negative selection pressure and making downstream data interpretation challenging. It has indeed been demonstrated in these screens that targeting of gRNAs to functional protein domains substantially increases the potency of negative selection, as these in-frame mutations are structurally unlikely to be tolerated[7]. In direct contrast to the consensus that retention of in-frame variants in true genetic dependencies is unwanted and confounds data interpretation in a CRISPR screen, we show here how selection of in-frame functional variants following CRISPR/Cas9 editing can in fact be exploited as an identification tool for genetic cancer dependencies. We label this methodology **CRISPR**/Cas9-mediated **N**egative-**S**election **I**dentification of genetic **D**ependencies (**CRISPR-NSID)**. CRISPR-NSID employs multiplex CRISPR/Cas9 for identification of genetic dependencies, *via* concomitant CRISPR/Cas9-mediated editing of tumor suppressor genes and genes mediating putative genetic dependencies. When targeting a factual genetic dependency, the imposed Darwinian selection mechanisms will result in retention of a higher-than-expected frequency of in-frame mutations in developing tumors. We show how this phenomenon can be exploited to identify genetic dependencies via binomial probability statistics, integrating known *a priori* probabilities of in-frame editing occurring in absence of selection pressure.

We had previously shown that targeting the mutation cluster region (MCR) of the *adenomatous polyposis coli* (*apc*) gene by TALENs allowed accurate modeling of desmoid tumors/desmoid-type fibromatosis associated with the familial adenomatous polyposis (FAP) syndrome in *Xenopus tropicalis* (*X. tropicalis*)[8]. Clinically, desmoid tumors are associated with either activating mutations in the *CTNNB1*

gene, which encodes β-catenin, or with biallelic *APC* mutations and are a frequent cause of FAP patient morbidity[9]. Since there is no evidence-based consensus treatment for desmoid tumors, there is a large unmet clinical need for targeted therapeutic agents in this tumor entity[10]. Desmoid tumors are considered purely monoclonal and non-metastasizing tumors, as such we reasoned this tumor type to be uniquely positioned to employ CRISPR-NSID for identification of dependency factors. In fact, tumors can be easily sampled as monoclonal outgrowths in *Xenopus* cancer models favoring straightforward genetic analysis[11]. In this study, we use CRISPR-NSID to identify EZH2 and CREB3L1 as novel dependency factors for desmoid tumors. Furthermore, we demonstrate that chemical inhibition of EZH2 can generate a therapeutic response in established desmoid tumors in our *apc* CRISPR/Cas9-driven tumor model, thereby creating an incentive for future pre-clinical studies.

Results

apc tumor suppressor gene inactivation initiates desmoid tumorigenesis in *Xenopus tropicalis*

We previously demonstrated penetrant induction of desmoid tumors (DT) by tissue-restricted TALENs-mediated genome engineering of *apc* in the anterior endoderm[8]. In the meanwhile, the advent of multiplex CRISPR/Cas9 for parallel gene inactivation pruned us to investigate whether DTs could similarly be induced by CRISPR/Cas9, in order to facilitate further downstream multiplexed gene inactivation studies[12]. We performed CRISPR/Cas9-mediated genome engineering of *apc*, in transgenic 8-cell embryos carrying a Wnt/β-catenin reporter construct[13] (Table S1a). Mosaic mutant F0 animals, further called crispants, presented with fully penetrant (100%; n=10) multiple desmoid tumors demonstrating active Wnt signaling and relevant histopathological hallmarks (Fig. S1a-c). Finally, targeted amplicon sequencing of a DT revealed positive selection for biallelic CRISPR/Cas9-induced *apc* frame shifting INDEL mutations (Table S1b). Interestingly, we also generated animals with a germline heterozygous one base pair deletion in the mutation cluster region (MCR) of the *apc* gene ($apc^{MCR/+}$), which similarly developed DTs (Fig. S1d) resembling the clinical presentation of FAP patients.

Identifying potential desmoid tumor genetic dependencies by a gene expression signature and literature mining

To compile a list of possible genetic dependencies desmoid tumors, we re-analyzed previously published transcriptomics studies to identify genes that are consistently upregulated in desmoid tumors compared to other fibrotic lesions[14,15]. We identified 251 genes that were over-expressed in DTs in two

independent datasets. Gene Set Enrichment Analysis revealed the Wnt signaling network to be amongst the top enriched pathways (adjusted $p < 0.001$) and showed that transcription factors are the most overrepresented gene family in DTs (16/251 genes) (Table S2). According to the ARCHS4 database, *CREB3L1* was the most significant transcription factor, expression of which highly correlated with expression levels of 58/251 genes that were upregulated in DTs (adjusted $p = 1.34 \times 10^{-49}$). We further mined the literature for genes previously shown to be associated with DT or previously associated with oncogenic processes. Additionally, we focused our efforts on genes for which the protein product was expected to be druggable in order to facilitate rapid clinical translation via drug repurposing approaches. As such we compiled the following putative dependency factors for essentiality screening in *apc* biallelic truncation-driven desmoid tumorigenesis: *hmmr*[16], *adam12*[17], *wisp-1*[18], *fap-α*[17], *mdk*[19], *nuak1*[20], *lox*[21], *pycr1*[22], *creb3l1*[23], *pclaf* and *ezh2*[24] (Table S3).

CRISPR-NSID identifies *ezh2* and *creb3l1* as genetic dependencies for desmoid tumors

We devised a strategy to identify genetic dependencies for desmoid tumors (i.e. potential targets for therapy) by multiplex CRISPR/Cas9 genome editing. We assumed that, if a gene is essential for DT development, there will be selection pressure to prevent tumor outgrowth in the absence of this dependency factor. This implies that, upon simultaneous *in vivo* CRISPR/Cas9-mediated editing of *apc* and a true dependency gene, biallelic frameshift mutations in this dependency gene will never be observed when performing genomic analysis of DTs sampled from these crispant animals. We first validated putative dependency factor (PuDF) gRNAs for high-efficiency genome editing upon unilateral or bilateral injection in two-cell *X. tropicalis* embryos (Table S1c). Next, we performed CRISPR-NSID by performing concomitant genome engineering, in vegetal-dorsal blastomeres, in *apc* and each of the eleven selected PuDF genes (Table S1d). For nine PuDFs (85%, n=11), we were able to recover desmoid tumors, sampled in post-metamorphic animals, containing biallelic frameshift mutations, indicating tumor occurrence in absence of functional PuDF protein product. This was the case for *lox*, *adam-12*, *mdk*, *hmmr*, *wisp1*, *nuak1*, *fap*-α, *pclaf* and *pycr1* (Fig. 1a, Table 1, Table S4). In contrast, we never sampled DTs with biallelic frameshift mutations in *ezh2,* targeted at serine 692 (*ezh2*^{S692}) and *creb3l1*, targeted at leucine 207 (*creb3l1*^{L207}) (Fig. 1a , Table 1, Table S4). The incapability of recovering DTs containing *ezh2*^{S692} or *creb3l1*^{L207} biallelic frameshift mutations is the consequence of the negative selection pressure that counter selects development of desmoid tumors lacking functional Ezh2 or Crebl3l1 protein. However, akin to *in vitro* CRISPR/Cas9 screens, this pressure does not manifest itself as complete absence of CRISPR/Cas9 editing in *ezh2*^{S692} or *creb3l1*^{L207}, but in fact exposes a higher-than-

expected rate of in-frame mutations that most likely retain protein functionality. In fact, biallelic mutations in *ezh2*^{S692} and *creb3l1*^{L207} in desmoid tumors could readily be recovered, but a clear mutational signature emerged in which each tumor retained at least one wild-type or in-frame allele. Evidently, we needed to verify that the incapability of recovering desmoid tumors carrying biallelic frameshift mutations in *ezh2*^{S692} or *creb3l1*^{L207} is not simply the consequence of under sampling, but rather reflects underlying negative selection mechanisms. In fact, it could be otherwise reasoned that not enough tumors were sampled to identify those carrying biallelic frameshift mutations, especially considering that we are dealing with mosaic edited animals. Therefore we devised a binomial statistics driven methodology using *a priori* probability of recovering biallelic frameshift mutations in a biallelic mutant DT and subjecting these expectations to real-life desmoid tumor sequencing data. For the frogs from the *apc/ezh2*^{S692} and *apc/creb3l1*^{L207} cohorts from which DTs were sampled, we also extracted DNA from the heart, an organ also receiving significant contribution from the injected dorsal-vegetal blastomeres, and performed genetic analysis of the *ezh2*^{S692} and *creb3l1*^{L207} loci. This provided us with an experimentally determined CRISPR/Cas9 INDEL scarring pattern for the employed gRNAs in each heart and allowed determination of the average frequency of frameshift mutations occurring across all hearts, in the absence of selection mechanisms. As such, we determine the average probability of **frameshift** editing for the *ezh2*^{S692} and *creb3l1*^{L207} gRNAs (*p*Frameshift). Obtaining this experimentally determined probability allows approximation of the probability of co-occurring **biallelic frameshift** mutations in a single desmoid tumor (*p*Frameshift^2). As such we can calculate the binomial probability that for a sampled number of **biallelic** mutant tumors, we never sample a **biallelic frameshift** mutant tumor. Using this methodology, we calculated the average probability of *ezh2*^{S692} and *creb3l1*^{L207} frameshift mutations occurring in hearts and used these to calculate the probability of observing a **biallelic frameshift** mutation in a desmoid tumor (Table S5a-f). The binomial probability of never observing **biallelic frameshift** mutations in the sampled **biallelic mutant** desmoid tumors is smaller than the 5% chance cutoff for *ezh2*^{S692} (p=0.033; n=4) (Fig. 1b) and *creb3l1*^{L207} (p=0.015; n=4) (Table S5c, f). Hence, the chance of never observing *ezh2*^{S692} or *creb3l1*^{L207} biallelic frameshift mutations in four biallelic mutant desmoid tumors, given the *a priori* probability for frameshift editing events obtained from hearts, is 3.3% and 1.5%, respectively, and therefore binomially unlikely. This never occurs in practice so that each desmoid tumor, as a consequence of Darwinian negative selection mechanisms, retains at least one wild type or functional in-frame allele for *ezh2* and *creb3l1*.

Interestingly, it was shown recently that double strand break repair by Non-Homologous End Joining upon template-free Cas9 editing is much less random than previously assumed and the INDEL pattern

can be predicted by using the inDelphi bio-informatics tool[25]. We used inDelphi to generate *in silico* predictions and found indeed correlation between inDelphi predicted INDEL scarring patterns and the experimentally obtained INDEL signature from *X. tropicalis* hearts for *ezh2*^{S692} (r_s=0.819, p<0.001) and *creb3l1*^{L207} (r_s=0.807, p<0.001) gRNAs (Table S6a). Again employing CRISPR-NSID binomial statistics as described before, we show that the binomial probabilities of never encountering biallelic frameshift mutations in the sampled biallelic mutant tumors, to be unlikely for *creb3l1*^{L207} (p=0.032), but not for *ezh2*^{S692} (p=0.054) (Fig. 2b) (Table S5c, f). Taken together, CRISPR-NSID reveals that genetic disruption of *lox*, *adam-12*, *mdk*, *hmmr*, *wisp1*, *nuak1*, *fap*-α, *pclaf* and *pycr1* does not prevent desmoid tumor development. While in direct contrast, we can never sample desmoid tumors with *ezh2* or *creb3l1* biallelic frameshift mutations but instead recover a statistically significant higher-than-expected ratio of in-frame mutations, indicating a dependency of desmoid tumors on Ezh2 and Creb3l1 protein.

In-frame *ezh2* mutations observed in desmoid tumors encode functional Ezh2 protein variants

Next, we sought to validate whether in-frame genetic variants, occurring upon *ezh2*^{S692} gRNA editing, encode Ezh2 protein variants that retain expression and functionality, which is obligate if they are indeed genetic dependencies. We performed structural modeling revealing that the three deletion variants map within a loop region at the periphery of the EZH2 subunit (Fig. 2a). Further, analysis of the structure of *Anolis carolinensis* EZH2 (*ac*EZH2) within the PCR2 complex assembled from human EED, human SUZ12-VEFS, and *Ac*EZH2 reveals that all three deletion variants would be expected to be well tolerated structurally[26]. Please note here the significant conservation of sequence identity between *human* EZH2, *Ac*EZH2 and *X. tropicalis* Ezh2 (Fig. 2a). Next, we performed expression studies introducing these EZH2 protein variants, as C-terminal Myc-tagged proteins, in *Xenopus tropicalis* embryos and HEK293T cells. We included in all expression assays, as a positive control, an Ezh2(p.Y643F) gain-of-function variant, corresponding to human EZH2(p.Y641F) that has been shown to increase histone 3 lysine 27 trimethylation activity relative to wild-type Ezh2[27]. In the *Xenopus* embryo expression assay, all Ezh2 variant proteins could be readily detected, with the exception of the Ezh2(p.Lys658fs) variant that lacks the C-terminal Myc-tag (Fig. 2b-top panel). Finally, in HEK293T cells we confirmed expression of all deletion variants and demonstrated their functionality in the PRC2 complex, by showing increased H3K27me3 levels upon overexpression of these Ezh2 protein variants (Fig. 2b-bottom panel). Taken together, we document that in-frame variants occurring in desmoid tumors upon *ezh2*^{S692} editing, encode EZH2 protein variants that retain expression and functionality.

Desmoid tumors have a genetic dependency on members of the polycomb repressive complex 2 (PRC2)

EZH2 inhibition is rapidly gaining traction as a therapeutic strategy and preclinical studies have shown promising results in other cancer types[28]. Hence, we validated *ezh2* as a genetic dependency in desmoid tumors, ruling out potential *ezh2* gRNA off-targets influencing our conclusions, by performing a validation CRISPR-NSID with gRNAs targeting another region of *ezh2*. It was previously described that negative selection pressure in CRISPR screens increases dramatically when targeting specific protein domains driving the dependency[7], since small in-frame deletions are in most cases not tolerated in critical functional domains. Therefore, we designed a gRNA targeting the *ezh2* exon encoding the histone methyl transferase SET-domain of Ezh2 at valine 659 ($ezh2^{V659}$). Employing CRISPR-NSID with $ezh2^{V659}$, we observed profound selection pressure on retaining at least one wild-type non-edited allele in all desmoid tumors investigated (Table 2). Based on editing efficiencies of the $ezh2^{V659}$ gRNA, the chance of recovering thirteen tumors with none showing biallelic *ezh2* editing events is binomially highly unlikely ($p<0.01$) (Table S6b). Further, if PRC2-mediated methyltransferase activity is indeed essential for desmoid tumorigenesis, we expect SUZ12, another subunit of PRC2, to be similarly identifiable as a genetic dependency in desmoid tumor development, in line with previous work in neuroblastoma cells[2]. For this, we designed a gRNA targeting *suz12* at asparagine 338 ($suz12^{N338}$). We performed CRISPR-NSID revealing negative selection on biallelic *suz12* frameshift mutations using *a priori* experimental heart data ($p=0.048$; n=7) and InDelphi predictions ($p<0.01$; n=7) (Table 2, Table S1d, S4, S5g-i, S6a). Taken together, these experiments demonstrate that both *ezh2* and *suz12* are genetic dependencies during desmoid tumor development, with selection pressure specifically on the SET-domain of Ezh2, making a strong case for a dependency on functional PCR2 during desmoid tumorigenesis.

Simultaneous negative and positive selection mechanisms during desmoid tumorigenesis upon targeting both *ezh2* and *tp53.*

As a final extension to our CRISPR-NSID model, we performed triple multiplex parallel genome engineering of *apc*, $ezh2^{V659}$ and *tp53* (Table 2, Table S1d, S6c)[29]. Interestingly, all desmoid tumors (n=8) sampled in this cohort demonstrated biallelic *tp53* editing, an event calculated as binomially unlikely ($p<0.01$) based on editing efficiencies of the *tp53* gRNA (Table S6d). This includes four tumors exhibiting *tp53* biallelic **frameshift** mutations indicating complete loss of p53 protein. This is indicative of positive selection pressure for inactivating p53, in line with published work[30]. In contrast, once again none of these desmoid tumors presented with biallelic mutations in *ezh2* (n=8). This experiment therefore also

reveals that the necessity on retaining functional Ezh2 during desmoid tumor development, cannot be bypassed by inactivation of p53[31].

EZH2 inhibition as therapeutic approach for desmoid tumors

To further validate the clinical relevance of our findings, we investigated whether, in line with literature[32], desmoid tumors indeed retain PRC2 complex activity. First, we demonstrated in clinical human desmoid tumors nuclear EZH2 immunoreactivity (Fig. S3). Interestingly, another desmoid tumor dependency factor identified in this study, CREB3L1, is also expressed in these clinical samples (Fig. S3). Furthermore, we observed profound H3K27me3 immunoreactivity in *Xenopus* desmoid tumors obtained from a cohort of *apc* CRISPR/Cas9 injected animals (Fig. S3). We believe our data this far provide solid genetic evidence demonstrating a necessity for PRC2, and per extensions the histone methyltransferase activity of EZH2, during desmoid tumorigenesis. However, as most patients will present with established desmoid tumors, we intended to investigate the effects of chemical EZH2 inhibition (EZH2i) on established desmoid tumors occurring in *apc* crispants. For this we exposed desmoid-tumor-bearing *apc* crispants to either EZH2i, via 10µM tazemetostat (EZP-6438), or mock treatment (Fig. 3A). By immunoblotting we demonstrate a reduction of H3K27me3 in the liver of drug-exposed animals compared to mock-treated animals indicative of tazemetostat bioabsorption and effectivity in *Xenopus* (Fig. 3B). Examination of tumor growth revealed reduction or stasis in desmoid tumor size in the treatment arm, in contrast to sustained tumor growth in the control arm ($p < 0.05$) (Fig. 3C-D) (Table S6d). We performed histopathological analysis of H&E-stained sections and staining for markers of proliferation and apoptosis, but could not observe immediate differences between tumors of the treatment and the control arm (data not shown). However, it should be pointed out that DTs are very slowly growing, thereby obscuring the identification of proliferation and cell death characteristics. Taken together, our CRISPR-NSID pipeline discovered a novel therapeutic strategy for treatment of FAP-associated desmoid tumors that we believe warrants further pre-clinical investigation.

Discussion

Clonal cancer growth is an inherently Darwinian process, where genetic mutations that increase fitness are under positive selection pressure and mutations disfavoring fitness are under negative selection pressure. In this study, we employ CRISPR/Cas9 to investigate whether targeted inactivation of several putative dependency factors (PuDFs) is under Darwinian negative selection pressure during clonal outgrowth. Namely, if a tumor carries a factual genetic dependency on expression of a gene, it is

expected that it would never be possible to obtain such a tumor upon introduction of INDEL mutations that affect the expression or the function of the respective protein. We exploited this tumor evolutionary process to generate a methodology called **CRISPR**/Cas9-mediated **N**egative-**S**election **I**dentification of **D**ependencies (**CRISPR-NSID)**, hinging on negative selection pressure to retain in the CRISPR/Cas9 targeted PuDF genes mutational patterns that retain protein expression and function. Via CRISPR-NSID, we showed that the genes *adam-12*[18], *hmmr*[16], *wisp-1*[18], *fap-α*[17], *mdk*[19], *nuak1*[20], *pclaf*[24], *lox* and *pycr1* are not true genetic dependencies for this tumor entity. Note that this does not rule out their involvement in the desmoid tumor pathogenic process, but merely establishes that they are not essential for tumor initiation or growth. In contrast, we demonstrate, via CRISPR-NSID, that desmoid tumors have a dependency for expression of Creb3l1 and two subunits of the polycomb repressive complex (PRC2), Ezh2 and Suz12. Furthermore, another member of the PRC2 complex, Suz12, was also found to be indispensable for DT growth. As such, we postulate that EZH2 mediates H3K27me3-mediated gene silencing of certain factors that have anti-oncogenic roles in desmoid tumor formation. The identity of these factors remains at this time elusive, but we show that they do not critically depend on p53 activity[31]. Interestingly, it was previously shown that desmoid tumors usually retain H3K27me3 immunoreactivity and we document here that EZH2 is indeed expressed in clinical DT samples[32]. Adapting this newly identified genetic dependency to a new therapeutic strategy, we demonstrate that chemical Ezh2 inhibition via tazemetostat has the potential to drive established demoid tumors in regression. The mechanisms by which this occurs are presently unknown and warrant further investigation together with further studies on the role of EZH2 in human desmoid tumor cells and genetic mouse models. While large scale AAV-mediated *in vivo* CRISPR screens in mouse cancer models have already been performed[33], these usually are dependent on a positive selection stimulus as negative selection pressure is much harder to ascertain. Namely, the absence of biallelic frameshift editing in tumors can always be attributed to the lack of sufficient sampling or insufficient genome editing, unless there are well-enforced *a priori* predictions of the expected genome editing outcomes and validation that sufficiently efficient genome editing indeed occurred. In this study we show that CRISPR-NSID is a rapid methodology for identification of novel genetic dependencies in an *in vivo* context. In fact, much akin to negative selection CRISPR screens in cell culture systems, both genetic dependency identification and concomitant elucidation of protein domains driving these dependencies are possible[7]. We show that the negative selection pressure during tumorigenesis on true genetic dependencies results in the recovery of specific in-frame variants encoding mutant proteins retaining expression and functionality. We expect CRISPR-NSID to be applicable across a wide range of cancers and to be further adaptable to

other model systems where CRISPR/Cas9 multiplexing can be easily achieved, such as zebrafish or tumor organoid culture systems. Furthermore, this methodology could also be adaptable to target specific PuDFs, in a hypothesis driven setting, in established cancer mouse models. Namely, in these models PuDF CRISPR/Cas9 scarring patterns and selection for tumors retaining at least one functional in-frame mutant can be investigated. We further believe that the necessity to experimentally determine the CRISPR/Cas9 scarring patterns in absence of selection, in order to perform a CRISPR-NSID analysis could in exploratory setups be replaced by scarring prediction software tools such as inDelphi[25]. Namely, the advent of machine learning in scarring prediction software is expected to yield increasingly accurate predictions of scarring patterns under absence of selection pressure, which can be back correlated to experimental tumor data. As such, we expect the CRISPR-NSID methodology to be uniquely positioned for *in vivo* validation of genetic dependencies identified in negative selection CRISPR/Cas9 screens in cancer cell cultures or *in vivo* xenografts of the latter.

In synopsis, we generated a new and highly penetrant CRISPR/Cas9-mediated model for desmoid-type fibromatosis in *Xenopus tropicalis*. We subsequently employed this model for CRISPR-NSID, elucidating new genetic dependencies on EZH2 and CREB3L1 in desmoid tumors, for which the dependency on the functional PRC2 complex was further validated. Desmoid tumors are a major cause of morbidity in familial adenomatous polyposis patients[9], and we show here for the first time that EZH2 inhibition, via a well-tolerated drug already in clinical trials (Tazemetostat – EPZ6438)[28], could be a novel therapeutic treatment for recurrent desmoid tumors.

Material and Methods

Generating the *apc*$^{MCR/+}$ line

F0 *apc* mosaics generated by *apc* TALENs injection[8] were outcrossed with WT *X. tropicalis*, and offspring was genotyped to identify heterozygotes via heteroduplex mobility assay as described before[34]. One distinct band pattern on heteroduplex mobility analysis (HMA)[34], was determined, by deep amplicon sequencing and BATCH-GE, to be indicative of a one base pair deletion in *apc* and these animals were grouped and further raised for analysis.

gRNA design and generation

apc gRNA was designed with the Doench, Hartenian algorithm[35]. *Mdk, wisp-1, lox*, *adam-12*, *hmmr, nuak1*, *creb3l1, FAP*-α, *pclaf*^{s8}, *pclaf*^{G10}, *pycr1, Ezh2*^{R49}, *Ezh2*^{S692}, *Ezh2*^{V659}, *tp53* and *suz12* gRNAs were

designed with the CRISPRScan software package[36]. *tp53* gRNA was generated as described before[29]. *In vitro* transcription, purification and quality control of injection-ready gRNA was performed as described before (Table S7a)[11].

DNA extraction and targeted deep sequencing

In order to analyze CRISPR/Cas9 genome editing efficiencies, tadpoles, tissue or tumors were incubated overnight at 55 °C in lysis buffer (50 mM Tris pH 8.8, 1 mM EDTA, 0.5% Tween-20, 200 µg/ml proteinase K). For assessing total genome editing efficiency for a specific injection setup we pooled nine stage 46 tadpoles before performing lysis. CRISPR/Cas9-target-site-containing amplicons were amplified by PCR with the primer pairs shown in Table S7b. Deep amplicon sequencing was performed with a validated pipe-line, INDEL frequency data and variant calling for all sequencing was performed with BATCH-GE bio-informatics analysis[37].

Generation of *X. tropicalis* mosaic mutants by CRISPR/Cas9

Wild-type *Xenopus tropicalis* females and males were primed with 20U and 10U PREGNYL© human chorionic gonadotropine (hCG) (Merck), respectively. Natural matings were set-up 2 days later, after boosting the female and male with 150U and 100U of hCG, respectively. Embryos were injected with the concentrations of RNP and within the blastomeres described in Table S7c. For all experiments we used NLS-Cas9-NLS (VIB Protein Service Facility, UGent), generated as described before[11]. All experiments were approved by the Ethical Committee for Animal Experimentation from Ghent University, Faculty of Science and VIB-Site Ghent. All methods were carried out in accordance with the relevant guidelines set out by this committee.

Differential expression analysis

In order to identify genes that are consistently upregulated in desmoid tumor fibromatosis compared to other fibrotic lesions, we re-analyzed the data from two previously published studies. The first dataset was generated by gene expression microarrays from 8 desmoid tumors, 10 dermatofibrosarcoma protuberans and 13 solitary fibrous tumors tumors[14]. The second dataset comprised 7 desmoid tumors compared to 9 different types of fibrous lesions that were profiled by 3SEQ[15]. We performed multiclass differential expression analyses using SAM for microarray data and SAMseq for 3SEQ data. We identified 251 genes (Table S2) that were upregulated in desmoid tumros in both datasets with contrast ≥2 and false detection rate ≤ 0.01. We performed functional annotation of these 251 genes using Gene Set

Enrichment Analysis (GSEA) (MSigDB, Molecular Signatures Database v6.2). Druggability was assessed via the DGIdb database[38].

CRISPR-NSID

For assessment of PuDF gRNA efficiencies, each gRNA was injected together with Cas9 recombinant protein as pre-complexed ribonucleoproteins (RNP), either unilaterally or bilaterally, in two-cell *X.* tropicalis embryos (Table S7c). Genome editing efficiencies were determined as described above. CRISPR-NSID was performed by multiplex CRISPR/Cas9, thus generating double crispants for both *apc* and respectively each of the eleven putative dependency factors (PuDF) under scrutiny. Genome editing efficiencies were determined as described above. Animals were further raised until post-metamorphosis. Please note that, considering the fluctuating *apc* editing efficiencies across setups, direct comparison of DT incidence rates to delineate impact of PuDF knockout on desmoid tumorigenesis is impossible. For each animal developing one or multiple desmoid tumors, targeted PCR amplicon sequencing was performed for the *apc* and the respective PuDF within the desmoid tumors and, in most cases, the heart. Noteworthy, the heart is a tissue receiving significant contribution from the vegetal-dorsal lineage and as such will serve as a proxy to determine the probability of frameshift mutations occurring for a specific gRNA in absence of selection pressure. In practice, each isolated desmoid tumor will have a varying content of non-neoplastic cells, which will be edited at basal efficiencies similar to the vegetal-dorsal lineage of the animal[6]. In order to perform a CRISPR-NSID analysis, we require monoclonal tumors and as such all tumors which showed more than two frequent mutation read variants in the *apc* gene were excluded from further analysis. PuDF were excluded as genetic dependencies when they demonstrated biallelic frameshift mutations in desmoid tumors. When we could never sample desmoid tumors containing biallelic frameshift mutations in desmoid tumors, but instead sampled a larger than expected amount of in-frame mutations, we performed binomial analysis to determine whether the probability of observing this was less than the binomial probability cut-off of 5% ($p < 0.05$). Based on the *a priori* determined (a) probability of frameshift mutations across the average of hearts (experimental) or (b) as predicted by inDelphi software[25] (*in silico* - https://indelphi.giffordlab.mit.edu/), we calculated the probabilities of co-encountering two frameshift (biallelic) mutations in biallelic mutant tumors (p). We then used binomial distribution to model the number of biallelic frameshift mutations in a tumor sample of size n with probability of occurrence p. Then, the probability of getting exactly k biallelic frameshift mutations in n tumors can then be written as $f(k,n,p) = \Pr(k,n,p) = \binom{n}{k} p^k (1-p)^{n-k}$. As an

example for *ezh2*^{S692}, with n = 4 and p = 0.573, the occurrence of zero (k) biallelic frameshift mutations across the tumors is 0.0331.

Imaging, histology and immunohistochemistry

Pictures of desmoid-tumor bearing animals, including the active Wnt signaling within desmoid tumors by dEGFP fluorescence, were taken with a Carl Zeiss StereoLUMAR.V12 stereomicroscope. *X. tropicalis* desmoid tumor tissue samples were harvested from benzocaine euthanized animals, fixed overnight at 4°C in 4% PFA, dehydrated and embedded in paraffin. Tissue sections were cut (5µm), stained and imaged as described before[11]. Clinical desmoid tumor samples were identified by D.C. and anonymized tissue sections were provided to perform immunofluorescence. Antigen retrieval was performed using a PickCell 2100-Retriever (ProteoGenix) in citrate buffer (10 mM citric acid, 0.1% Tween-20, pH 6). Slides were subsequently blocked with blocking buffer (3% natural serum, 1% BSA, 0.1% Tween-20) and incubated overnight with anti-EZH2 antibody (3748; Abcam), anti-CREB3L1 (AF4080; Rndsystems) or anti-H3K27me3 (07-449, Merck). Detection was performed with respectively goat anti-rabbit DyLight-594, donkey anti-goat DyLight-594 and goat anti-rabbit DyLight-633. Counterstaining was performed with Hoechst-33342 and sections were imaged using a Leica TCS LSI zoom confocal microscope.

Expression of EZH2 protein variants

C-terminal Myc-epitope-tagged expression plasmid pCS2-MT-EZH2 was generated by cloning *X. tropicalis ezh2* cDNA, excluding the stop codon, in-frame into the BamHI-ClaI sites of the pCS2-MT vector. Specific mutations, NM_00101793.2:c.2163_2180del; NM_001017293.2:c.2165_2182del; NM_001017293.2:c.2171_2179del; NM_001017293.2:c.2068_2074del; NM_001017293.2:c.2127A>T, were introduced in full-length *ezh2* cDNA by the Q5® Site-Directed Mutagenesis Kit (NEB; E0544S). Resulting plasmids were sequence validated by Sanger, digested with NotI and employed for SP6 *in vitro* transcription of *ezh2* variant mRNA. Two-cell *X. tropicalis* embryos were injected with 500 pg of capped mRNA and allowed to develop to stage 19 and cell extract was prepared in E1A lysis buffer (250 mM NaCl, 50 mM Tris pH 7.4, 0.1% NP-40) containing a complete protease inhibitor cocktail (1:25) (Roche) and centrifuged for 10 min at 14.000 r.p.m. in a microcentrifuge at 4 °C. Cleared supernatants, without yolk contamination, was further used. For transfection experiments, wells were seeded with 200.000 HEK293T cells and transfected the next day using CaCl2 transformation with 100 ng of each of the PCS2-MT-EZH2 plasmids or 100 ng pMAX-GFP plasmid transfection control together with 900 ng of PCS2-MT carrier plasmid. For two replicates cell extracts were prepared in RIPA buffer (25mM Tris-HCl pH 7.6,

150mM NaCl, 1% NP-40, 1% sodium deoxycholate, 0.1% SDS) containing complete HALT protease and phosphatase inhibitor cocktail (Pierce). For the third replica, cells were harvested in 1x PBS, centrifuged, resuspended and split in two. One part was used for cell extract preparation by RIPA as described before. The other part was used for histone extraction. Histone extracts were prepared as described before[39], the nucleus was first purified (1X PBS, 0.5% Triton X-100 and 5 mM sodium butyrate) followed by acid extraction (0.4 M HCl) for 1 h at 4 °C and finally the extract was neutralized with 2.5× of 1 M Na_2HPO_4. All protein extracts were denatured in laemmli buffer, separated by SDS-polyacrylamide gel electrophoresis (20 µg for total protein extracts and 1 µg for histone extracts) and transferred to PVDF. Following antibodies were used for immunodetection: anti-myctag (9106; Abcam), anti-β-actin-HRP (47778; Santa Cruz), anti-h3k27me3 (39155; Active-motif) and anti-total H3 (1791; Abcam).

***In vivo* EZH2 inhibition**

DT-bearing *apc* crispants were generated as described before. Ninety day old animals were randomly assigned to either the treatment or the control arm. Animals were kept in 0.1x MMR containing either 10 µM EPZ-6438 (HY-13803; MedChem Express)/0.0011% DMSO or 0.0011% DMSO. Every day, half of the 0.1x MMR, containing either EPZ-6438 or mock treatment, was refreshed. A baseline tumor photography was made using a Carl Zeiss StereoLUMAR.V12 stereomicroscope, and a second photograph was taken after 21 days of treatment. Tumor sizes were quantified using ImageJ and statistical analysis was performed using a Two-way ANOVA with repeated measures.

Acknowledgements

The authors would like to thank Arne Martens, Nicolas Skrypek and Marja Kreike for providing assistance with cell culture experiments. We would like to acknowledge Marjolein Carron and Lana Hellebaut for proof-reading and scientific discussions leading to new relevant insights.

References

1. Tsherniak, A. *et al.* Defining a Cancer Dependency Map. *Cell* **170,** 564–576.e16 (2017).
2. Chen, L. *et al.* CRISPR-Cas9 screen reveals a MYCN-amplified neuroblastoma dependency on EZH2. *J. Clin. Invest.* **128,** 446–462 (2017).
3. Tzelepis, K. *et al.* A CRISPR Dropout Screen Identifies Genetic Vulnerabilities and Therapeutic Targets in Acute Myeloid Leukemia. *Cell Rep.* **17,** 1193–1205 (2016).
4. Yamauchi, T. *et al.* Genome-wide CRISPR-Cas9 Screen Identifies Leukemia-Specific Dependence on a Pre-mRNA Metabolic Pathway Regulated by DCPS. *Cancer Cell* **33,** 386–400.e5 (2018).
5. Maresch, R. *et al.* Multiplexed pancreatic genome engineering and cancer induction by transfection-based CRISPR/Cas9 delivery in mice. *Nat. Commun.* **7,** (2016).

6. Weber, J. *et al.* CRISPR/Cas9 somatic multiplex-mutagenesis for high-throughput functional cancer genomics in mice. *Proc. Natl. Acad. Sci. U. S. A.* **112,** 13982–7 (2015).
7. Shi, J. *et al.* Discovery of cancer drug targets by CRISPR-Cas9 screening of protein domains. doi:10.1038/nbt.3235
8. Van Nieuwenhuysen, T. *et al.* TALEN-mediated apc mutation in Xenopus tropicalis phenocopies familial adenomatous polyposis. *Oncoscience* **2,** (2015).
9. de Campos, F. G. C. M. *et al.* Evaluating Causes of Death in Familial Adenomatous Polyposis. *J. Gastrointest. Surg.* **14,** 1943–1949 (2010).
10. Skubitz, K. M. Biology and Treatment of Aggressive Fibromatosis or Desmoid Tumor. *Mayo Clin. Proc.* **92,** 947–964 (2017).
11. Naert, T. *et al.* CRISPR/Cas9 mediated knockout of rb1 and rbl1 leads to rapid and penetrant retinoblastoma development in Xenopus tropicalis. *Sci. Rep.* **6,** (2016).
12. Naert, T., Van Nieuwenhuysen, T. & Vleminckx, K. TALENs and CRISPR/Cas9 fuel genetically engineered clinically relevant *Xenopus tropicalis* tumor models. *genesis* **55,** e23005 (2017).
13. Tran, H. T., Sekkali, B., Van Imschoot, G., Janssens, S. & Vleminckx, K. Wnt/beta-catenin signaling is involved in the induction and maintenance of primitive hematopoiesis in the vertebrate embryo. *Proc. Natl. Acad. Sci. U. S. A.* **107,** 16160–5 (2010).
14. West, R. B. *et al.* Determination of Stromal Signatures in Breast Carcinoma. *PLoS Biol.* **3,** e187 (2005).
15. Guo, X., Zhu, S. X., Brunner, A. L., van de Rijn, M. & West, R. B. Next generation sequencing-based expression profiling identifies signatures from benign stromal proliferations that define stromal components of breast cancer. *Breast Cancer Res.* **15,** R117 (2013).
16. Tolg, C., Poon, R., Fodde, R., Turley, E. A. & Alman, B. A. Genetic deletion of receptor for hyaluronan-mediated motility (Rhamm) attenuates the formation of aggressive fibromatosis (desmoid tumor). *Oncogene* **22,** 6873–6882 (2003).
17. Misemer, B. S. *et al.* Expression of FAP, ADAM12, WISP1, and SOX11 is heterogeneous in aggressive fibromatosis and spatially relates to the histologic features of tumor activity. *Cancer Med.* **3,** 81–90 (2014).
18. Skubitz, K. M. & Skubitz, A. P. . Gene expression in aggressive fibromatosis. *J. Lab. Clin. Med.* **143,** 89–98 (2004).
19. Colombo, C. *et al.* Increased midkine expression correlates with desmoid tumour recurrence: a potential biomarker and therapeutic target. *J. Pathol.* **225,** 574–582 (2011).
20. Port, J. *et al.* Colorectal Tumors Require NUAK1 for Protection from Oxidative Stress. *Cancer Discov.* **8,** 632–647 (2018).
21. Wang, T.-H., Hsia, S.-M. & Shieh, T.-M. Lysyl Oxidase and the Tumor Microenvironment. *Int. J. Mol. Sci.* **18,** (2016).
22. Reversade, B. *et al.* Mutations in PYCR1 cause cutis laxa with progeroid features. *Nat. Genet.* **41,** 1016–1021 (2009).
23. Chen, Q., Lee, C.-E., Denard, B. & Ye, J. Sustained Induction of Collagen Synthesis by TGF-β Requires Regulated Intramembrane Proteolysis of CREB3L1. *PLoS One* **9,** e108528 (2014).
24. Jung, H.-Y. *et al.* PAF and EZH2 Induce Wnt/β-Catenin Signaling Hyperactivation. *Mol. Cell* **52,** 193–205 (2013).
25. Shen, M. W. *et al.* Predictable and precise template-free CRISPR editing of pathogenic variants. *Nature* **563,** 646–651 (2018).
26. Brooun, A. *et al.* Polycomb repressive complex 2 structure with inhibitor reveals a mechanism of activation and drug resistance. *Nat. Commun.* **7,** 11384 (2016).
27. Souroullas, G. P. *et al.* An oncogenic Ezh2 mutation induces tumors through global redistribution of histone 3 lysine 27 trimethylation. *Nat. Med.* **22,** 632–640 (2016).
28. Morschhauser, F. *et al.* Phase 2 multi-center study of tazemetostat (EPZ-6438), an inhibitor of enhancer of zeste-homolog 2 (EZH2), in patients with relapsed or refractory B-cell non-Hodgkin lymphoma (NHL). *J. Clin. Oncol.* **34,** TPS7582-TPS7582 (2016).
29. Naert, T. *et al.* RBL1 (p107) functions as tumor suppressor in glioblastoma and small-cell pancreatic neuroendocrine carcinoma. *bioRxiv* 528299 (2019). doi:10.1101/528299
30. Smits, R. *et al.* Apc1638N: a mouse model for familial adenomatous polyposis-associated desmoid tumors and cutaneous cysts. *Gastroenterology* **114,** 275–83 (1998).

31. Chen, Q., Zheng, P.-S. & Yang, W.-T. EZH2-mediated repression of GSK-3β and TP53 promotes Wnt/β-catenin signaling-dependent cell expansion in cervical carcinoma. *Oncotarget* **7,** 36115–36129 (2016).
32. Mito, J. K., Qian, X., Doyle, L. A., Hornick, J. L. & Jo, V. Y. Role of Histone H3K27 Trimethylation Loss as a Marker for Malignant Peripheral Nerve Sheath Tumor in Fine-Needle Aspiration and Small Biopsy Specimens. *Am. J. Clin. Pathol.* **148,** 179–189 (2017).
33. Chen, S. *et al.* Genome-wide CRISPR screen in a mouse model of tumor growth and metastasis. *Cell* **160,** 1246–60 (2015).
34. Naert, T. & Vleminckx, K. in *Methods in molecular biology (Clifton, N.J.)* **1865,** 67–82 (2018).
35. Doench, J. G. *et al.* Rational design of highly active sgRNAs for CRISPR-Cas9–mediated gene inactivation. (2014). doi:10.1038/nbt.3026
36. Moreno-Mateos, M. A. *et al.* CRISPRscan: designing highly efficient sgRNAs for CRISPR-Cas9 targeting in vivo. *Nat. Methods* **12,** 982–8 (2015).
37. Boel, A. *et al.* BATCH-GE: Batch analysis of Next-Generation Sequencing data for genome editing assessment. *Sci. Rep.* **6,** 30330 (2016).
38. Cotto, K. C. *et al.* DGIdb 3.0: a redesign and expansion of the drug–gene interaction database. *Nucleic Acids Res.* **46,** D1068–D1073 (2018).
39. Skrypek, N. *et al.* ZEB2 stably represses RAB25 expression through epigenetic regulation by SIRT1 and DNMTs during epithelial-to-mesenchymal transition. *Epigenetics Chromatin* **11,** 70 (2018).

Figure and Table Legends

Figure 1: CRISPR-NSID pipeline reveals that, when concomitantly targeting *apc* and one of eleven putative dependency factors (PuDF), desmoid tumors critically depend on expression of Ezh2 and Creb3l1. (a) Targeting *apc* and a *PuDF* by multiplex CRISPR/Cas9 induces desmoid tumors of which the percentage carrying biallelic frameshift mutations in the *PuDF* is shown in the graph. Note that we never observe biallelic frameshift mutations in either *ezh2* or *crebl3l1* in desmoid tumors. **(b)** Schematic representation of the CRISPR-NSID methodology as run for the *ezh2*^{S692} dataset (See also Table 1). In the *apc/ezh2*^{S692} cohort we obtained eight desmoid tumors, in which four exhibited biallelic mutations. None of these exhibited biallelic frameshift mutations. Using experimental data obtained from sequencing hearts in the *apc/ezh2*^{S692} cohort, we predict the chance of biallelic frameshift mutation in any given desmoid tumor to be 57.34%, as such the probability of sampling zero biallelic frameshift mutations in four biallelic mutant tumors is 3.31% ($p<0.05$). Using the inDelphi tool, we predict the chance of biallelic frameshift mutation in any given desmoid tumor to be 51.84%, as such the probability of sampling zero biallelic frameshift mutations in four biallelic mutant tumors is 5.38%.

Figure 2: In-frame *ezh2* mutations observed in desmoid tumors encode functional Ezh2 protein variants. (a**)** Mapping of identified deletion mutations in the EZH2 subunit of the polycomb repressive complex 2 (PCR2). The structural template shown is based on pdb entry 5IJ7[26]. Ezh2 from *Xenopus tropicalis* shares 96% sequence identity with the *Ac*EZH2 used to assemble this structural template. Further are the regions containing mutations 100% conserved between human EZH2, *X. tropicalis* Ezh2 and *Ac*EZH2 (See alignment). The deletion variants occur in a loop at the periphery of the Ezh2 subunit and are expected to be well tolerated structurally. **(b)** Expression studies of Ezh2 protein variants. In-frame deletions variants, obtained from genetic analysis of desmoid tumors, were expressed in two systems to investigate expression levels and functionality. **(Top)** Immunoblot from embryo lysates (st. 19), injected at two cell stage with capped mRNA coding for an Ezh2 protein variants containing a C-terminally Myc-tag. Myc immunoblotting was noted for all protein variants except for the Ezh2(p.Lys658fs) frameshift negative control that lacks the C-terminal Myc tag. Actin is shown as loading control. **(Bottom)** Plasmids carrying the coding sequences for either wild-type Ezh2, variant mutant Ezh2 or gain-of-function Ezh2(p.Y643F) were transfected in HEK293T cells. pMaxGFP was also transfected as transfection control. Myc immunoblotting is noted for WT Ezh2 and all Ezh2 protein variants, except for the Ezh2(p.Lys658fs) or the pMaxGFP transfection control. Actin is shown as loading control. Data are representative of three independent experiments. Further, histone extracts were analyzed by

immunoblotting revealing an increase in the levels of H3K27me3 upon overexpression of wild-type Ezh2 or Ezh2(p.Y643F) (white arrowheads), when compared to the transfection control (black arrowhead). For Ezh2 protein variants we demonstrate that functionality as they increase H3K27me3 compared to the transfection control. Total H3 is shown as loading control. Immunoblots were cut and pasted (see white space in blots). Unaltered original scans of blots are shown in Supplementary Fig. S2.

Figure 3: Tazemetostat treatment of animals carrying established DTs upon *apc* inactivation leads to reduction in tumor size. (A) 90 days old *apc* crispants with established DTs (n=10) were split equally across either a treatment (10 µM tazemetostat) or a control (DMSO) arm for 21 days, with daily change of compound or DMSO containing housing water. **(B)** Western blot demonstrates that tazemetostat-exposed animals, but not DMSO-exposed animals, show a reduction in H3K27me3 levels in the liver, demonstrating absorption of the compound from the housing water. Unaltered original scans of blots are shown in Supplementary Fig. S2. **(C)** Representative picture demonstrating a regressing desmoid tumor in the 10 µM tazemetostat treatment arm. Insets are higher magnification pictures of the DT, before and after treatment. **(D)** Measuring of DT size reveals stable or progressive disease in the control arm, while only in tazemetostat-exposed animals regression or stasis of tumor could be observed. Each data-point represents one desmoid tumor, note that some animals developed several tumors. Two-way ANOVA with Repeated measures showed that treatment had a significant effect (p = 0.013) on tumor sizes. ANOVA table is listed in Table S6D. *P < 0.05

Table 1: CRISPR-NSID reveals dependency on functional Ezh2 and Creb3l1 during *apc* biallelic truncation driven desmoid tumorigenesis. Desmoid tumors are in all cases driven by biallelic out-of-frame INDEL mutations in the *apc* gene (note that some DTs carry identical mutations on both alleles). Furthermore, tumors carrying biallelic frameshift mutations in *lox*, *adam12*, *mdk*, *hmmr*, *wisp1*, *nuak1*, *FAP*-α, *pclaf* and *pycr1* were sampled. Tumors carrying these biallelic frameshift mutations are highlighted in grey. In contrast, biallelic frameshift editing was never sampled for *ezh2* or *creb3l1*, due to negative selection pressure on retention of functional Ezh2 and Crebl3l1 during desmoid tumorigenesis.

Table 2: CRISPR-NSID reveals dependency on functional Ezh2 and Suz12 and positive selection for biallelic *tp53* mutations during *apc* biallelic truncation driven desmoid tumorigenesis. Desmoid tumors are in all cases driven by biallelic mutations in the *apc* gene, of which some DTs carry identical mutations on both alleles. Biallelic frameshift editing never was never sampled in *ezh2* or *suz12*, due to negative selection pressure leading to retention of functional Ezh2 and Suz12 during desmoid tumorigenesis. Further, in a triple multiplex CRISPR/Cas9 editing contrast, *tp53* biallelic mutations were readily

discovered in desmoid tumors and are under positive selection pressure ($p < 0.01$ – Table S6d), while once again biallelic frameshift editing was never sampled in *ezh2* .

Figure 1

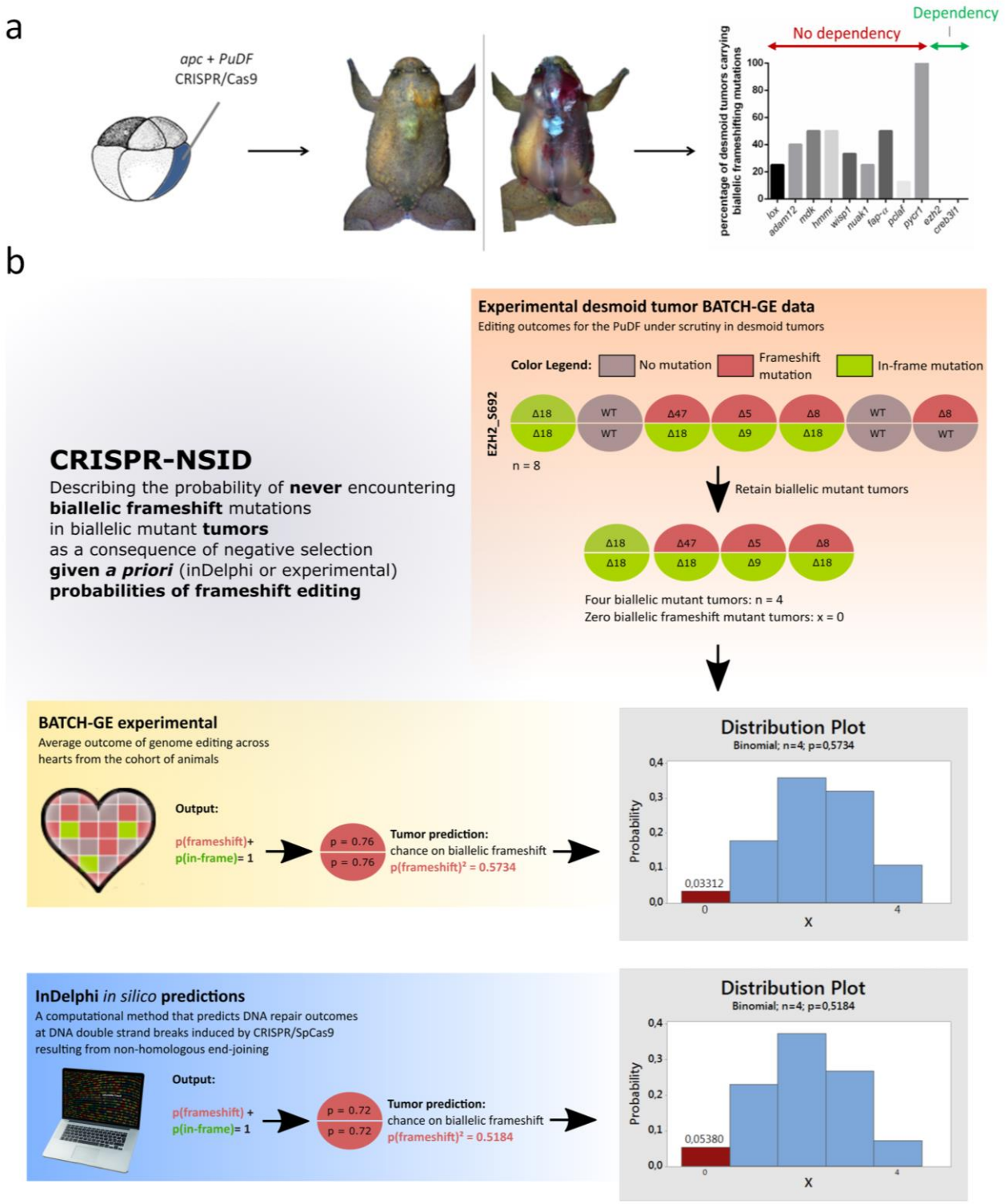
a
apc + PuDF
CRISPR/Cas9
Dependency
No dependency
percentage of desmoid tumors carrying biallelic frameshifting mutations
100
80
60
40
20
0
lox
adam12
mdk
hmmr
wisp1
nuak1
fap-a
pclaf
pycr1
ezh2
creb3l1
b
CRISPR-NSID
Describing the probability of never encountering biallelic frameshift mutations in biallelic mutant tumors as a consequence of negative selection given a priori (inDelphi or experimental) probabilities of frameshift editing
Experimental desmoid tumor BATCH-GE data
Editing outcomes for the PuDF under scrutiny in desmoid tumors
Color Legend:
No mutation
Frameshift mutation
In-frame mutation
EZH2_S692
Δ18 Δ18
WT WT
Δ47 Δ18
Δ5 Δ9
Δ8 Δ18
WT WT
Δ8 WT
n = 8
Retain biallelic mutant tumors
Δ18 Δ18
Δ47 Δ18
Δ5 Δ9
Δ8 Δ18
Four biallelic mutant tumors: n = 4
Zero biallelic frameshift mutant tumors: x = 0
BATCH-GE experimental
Average outcome of genome editing across hearts from the cohort of animals
Output:
p(frameshift)+
p(in-frame)= 1
p = 0.76
p = 0.76
Tumor prediction:
chance on biallelic frameshift
p(frameshift)² = 0.5734
Distribution Plot
Binomial; n=4; p=0,5734
Probability
0,4
0,3
0,2
0,1
0,0
0,03312
0
4
X
InDelphi in silico predictions
A computational method that predicts DNA repair outcomes at DNA double strand breaks induced by CRISPR/SpCas9 resulting from non-homologous end-joining
Output:
p(frameshift) +
p(in-frame)= 1
p = 0.72
p = 0.72
Tumor prediction:
chance on biallelic frameshift
p(frameshift)² = 0.5184
Distribution Plot
Binomial; n=4; p=0,5184
Probability
0,4
0,3
0,2
0,1
0,0
0,05380
0
4
X

Figure 2

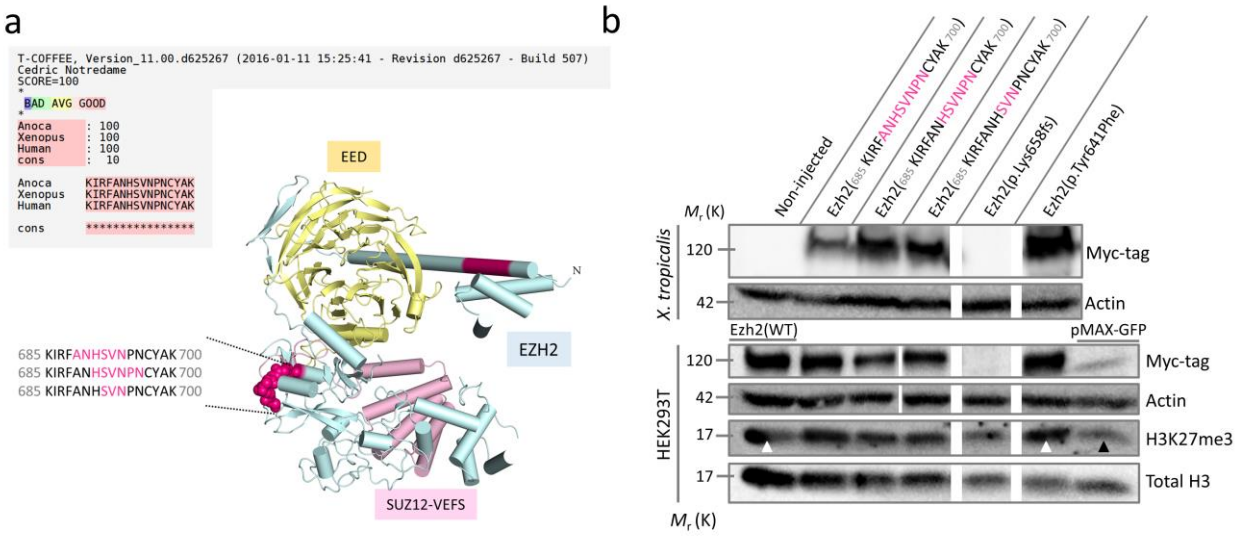
a
T-COFFEE, Version_11.00.d625267 (2016-01-11 15:25:41 - Revision d625267 - Build 507)
Cedric Notredame
SCORE=100
BAD AVG GOOD
Anoca : 100
Xenopus : 100
Human : 100
cons : 10
Anoca KIRFANHSVNPNCYAK
Xenopus KIRFANHSVNPNCYAK
Human KIRFANHSVNPNCYAK
cons **********
EED
EZH2
SUZ12-VEFS
685 KIRFANHSVNPNCYAK 700
685 KIRFANHSVNPNCYAK 700
685 KIRFANHSVNPNCYAK 700
b
Non-injected
Ezh2(685 KIRFANHSVNPNCYAK 700)
Ezh2(685 KIRFANHSVNPNCYAK 700)
Ezh2(685 KIRFANHSVNPNCYAK 700)
Ezh2(p.Lys658fs)
Ezh2(p.Tyr641Phe)
Mr (K)
X. tropicalis
120
42
Myc-tag
Actin
Ezh2(WT)
pMAX-GFP
HEK293T
120
42
17
17
Myc-tag
Actin
H3K27me3
Total H3
Mr (K)

Figure 3

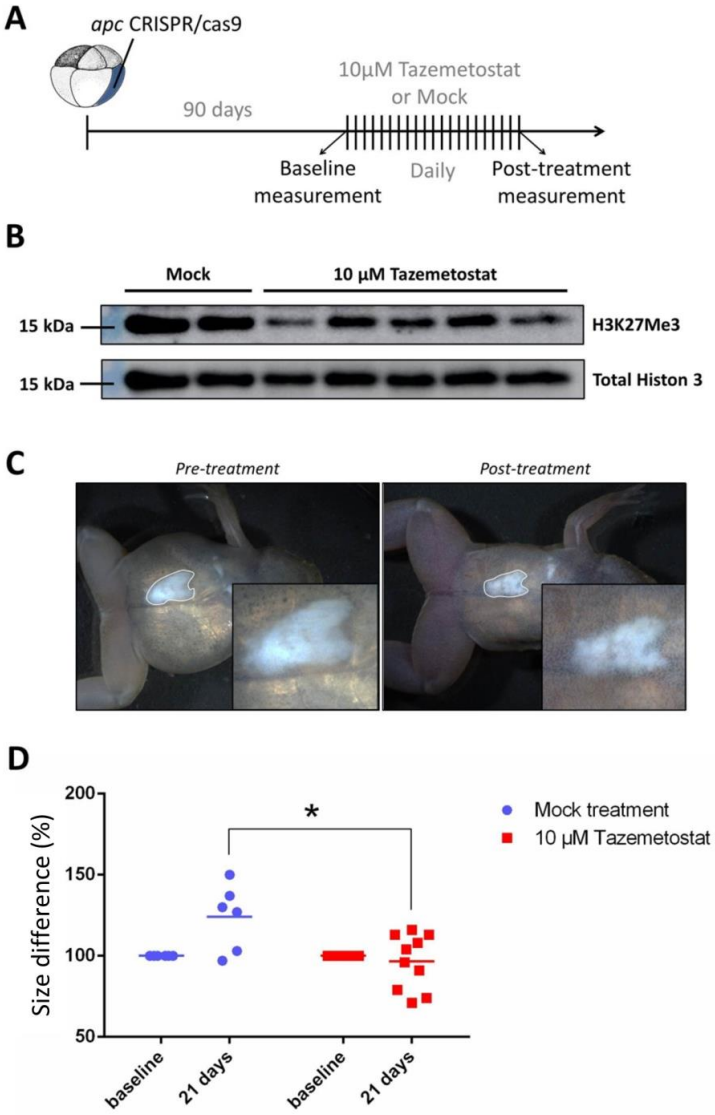
A
apc CRISPR/cas9
90 days
10µM Tazemetostat
or Mock
Baseline
measurement
Daily
Post-treatment
measurement
B
Mock
10 µM Tazemetostat
15 kDa
H3K27Me3
15 kDa
Total Histon 3
C
Pre-treatment
Post-treatment
D
Size difference (%)
200
150
100
50
*
Mock treatment
10 µM Tazemetostat
baseline
21 days
baseline
21 days

Table 1

lox

	apc	*lox*
Tumor 1	Δ4, +1	Δ22, +1
Tumor 2	+1 and +1, +1	Δ21
Tumor 3	Δ7, +1	Δ21, Δ5
Tumor 4	Δ7, +1	Δ23, Δ5, +1

adam12

	apc	*adam12*
Tumor 1	Δ4, +1	Δ6, Δ1
Tumor 2	Δ4, +1	Δ7
Tumor 3	Δ7, Δ10	Δ3
Tumor 4	Δ7, Δ4	Δ4, Δ13 (+1 with Δ14)
Tumor 5	Δ7, Δ2	Δ14, +2
Tumor 6	Δ7, Δ2	
Tumor 7	Δ5, Δ2	Δ10
Tumor 8	Δ5	Δ10
Tumor 9	Δ6, +1	Δ8, Δ3
Tumor 10	Δ7	Δ7, Δ8

mdk

	apc	*mdk*
Tumor 1	Δ7, Δ1	Δ13, Δ14
Tumor 2	Δ7, Δ4	Δ9, Δ12
Tumor 3	Δ7, Δ1	Δ14, Δ14
Tumor 4	Δ4 with +1, Δ7	Δ12
Tumor 5	Δ4, +1	Δ13, +1
Tumor 6	Δ4, +1	Δ36, +10 (+7 with Δ9 and +12)

hmmr

	apc	*hmmr*
Tumor 1	Δ31, +1	Δ13, Δ7
Tumor 2	+1, +2	Δ6
Tumor 3	Δ7, +1	Δ7, Δ1
Tumor 4	Δ7, +1	Δ6

wisp1

	apc	*wisp1*
Tumor 1	Δ16, Δ4	Δ7, Δ4, Δ2
Tumor 2	Δ5, +1	
Tumor 3	Δ7, Δ20	

nuak1

	apc	*nuak1*
Tumor 1	Δ5, Δ4	Δ4, Δ1
Tumor 2	Δ5, +5	Δ22
Tumor 3	Δ7	Δ4
Tumor 4	Δ7, Δ4	Δ27, Δ9
Tumor 5	Δ8	Δ55, Δ11
Tumor 6	Δ8 with +11, Δ7	Δ17, +24
Tumor 7	Δ2, +14	Δ12, +3
Tumor 8	Δ4	Δ21

fap-α

	apc	*fap-α*
Tumor 1	Δ7, Δ4	Δ17, Δ1
Tumor 2	1, +7	Δ29
Tumor 3	Δ7, Δ4	Δ7, Δ2
Tumor 4	Δ7, Δ5	Δ1, +15

pclaf_S8

	apc	*pclaf_v1*
Tumor 1	Δ7	Δ6
Tumor 2	+2, +4	Δ6
Tumor 3	Δ5, +1	Δ1
Tumor 4	Δ7	Δ7
Tumor 5	Δ5, +6	
Tumor 6	Δ2, +1	Δ59
Tumor 7	Δ5, Δ4	1
Tumor 8	Δ7, +1	
Tumor 9	Δ7, +Δ4	Δ6, +1
Tumor 10	Δ7, +1	Δ12, +7
Tumor 11	+1	Δ12
Tumor 12	Δ23, Δ2	Δ4, Δ5

pclaf_G10

	apc	*pclaf_v2*
Tumor 1	Δ5, Δ4	
Tumor 2	+6, +13	
Tumor 3	Δ7, Δ5	
Tumor 4	Δ4, +16	
Tumor 5	Δ5, +2	
Tumor 6	Δ7, Δ4	Δ4, Δ4
Tumor 7	Δ7, Δ4	Δ4
Tumor 8	Δ7, +5 with Δ1	Δ13
Tumor 9	Δ4, Δ5, Δ8	Δ4, Δ1
Tumor 10	Δ4, +1	Δ1
Tumor 11	Δ4, +1	Δ1, Δ19
Tumor 12	Δ7, +1	Δ4, Δ9

pycr1

	apc	*pycr1*
Tumor 1	Δ7, +1	Δ20, Δ5
Tumor 2	Δ5, +1	Δ4, Δ5

ezh2_S692

	apc	*ezh2_S692*
Tumor 1	Δ4, +1	Δ18, Δ18
Tumor 2	Δ14, Δ7	
Tumor 3	Δ2, +8	Δ47, Δ18
Tumor 4	Δ4, Δ2	Δ5 (Δ2 with Δ3), Δ9
Tumor 5	Δ4, Δ5	Δ18, Δ8
Tumor 6	Δ7, Δ5	
Tumor 7	Δ7	Δ8

creb3l1

	apc	*creb3l1*
Tumor 1	Δ7, Δ6	
Tumor 2	Δ7, +1	Δ4
Tumor 3	+1, +4	Δ9, Δ5
Tumor 4	Δ1, +1	Δ7, Δ9
Tumor 5	Δ7, Δ2	Δ2, Δ3
Tumor 6	Δ5, Δ7 (Δ5 with Δ2)	Δ3
Tumor 7	Δ2, Δ5	+7
Tumor 8	Δ5, Δ5	Δ6
Tumor 9	Δ4, +7	Δ16, Δ3

Table 2

ezh2_V659

	apc	*ezh2_V659*
Tumor 1	Δ4, Δ2	Δ7
Tumor 2	Δ28, Δ7	Δ2
Tumor 3	Δ7, Δ4	Δ3
Tumor 4	Δ7, Δ5	Δ3
Tumor 5	Δ7, Δ4	Δ6
Tumor 6	Δ7, +1	
Tumor 7	Δ8	
Tumor 8	Δ4, +1	
Tumor 9	Δ7	Δ1
Tumor 10	Δ7, Δ2	
Tumor 11	Δ7, Δ4	Δ10
Tumor 12	Δ7, Δ2	
Tumor 13	Δ7, +19	+1
Tumor 14	Δ7, Δ2	Δ3
Tumor 15	Δ7, +1	Δ2
Tumor 16	Δ4, +1	+6
Tumor 17	Δ4, Δ5	

suz12_N338

	apc	*suz12_N338*
Tumor 1	+1	Δ7, Δ6
Tumor 2	Δ7, Δ5	Δ9, Δ8
Tumor 3	Δ7, Δ4	Δ5 (Δ4 with Δ6 and +5)
Tumor 4	Δ5	Δ19, Δ6
Tumor 5	Δ4, Δ11	Δ3
Tumor 6	Δ7	Δ1, +3
Tumor 7	Δ1, Δ2	
Tumor 8	Δ7, Δ2	Δ12, Δ19
Tumor 9	Δ7, Δ4	+5, Δ6 (+1 and Δ7)
Tumor 10	Δ4, Δ2	Δ6, Δ4
Tumor 11	Δ7, Δ4	Δ17

ezh2_V659 + tp53

	apc	*ezh2_V659*	*tp53*
Tumor 1	Δ4, +51 (+1 with Δ1 and +51)		Δ12, +2
Tumor 2	Δ7, +8		Δ10, Δ4
Tumor 3	+1		Δ4, Δ3, Δ3
Tumor 4	Δ7	Δ5	Δ4, Δ4
Tumor 5	+1	Δ6	Δ6, Δ4
Tumor 6	Δ5	Δ40	Δ4, Δ4
Tumor 7	+1	Δ6	Δ6, Δ4
Tumor 8	+1, +1	Δ4	Δ4, Δ4

Supplementary data

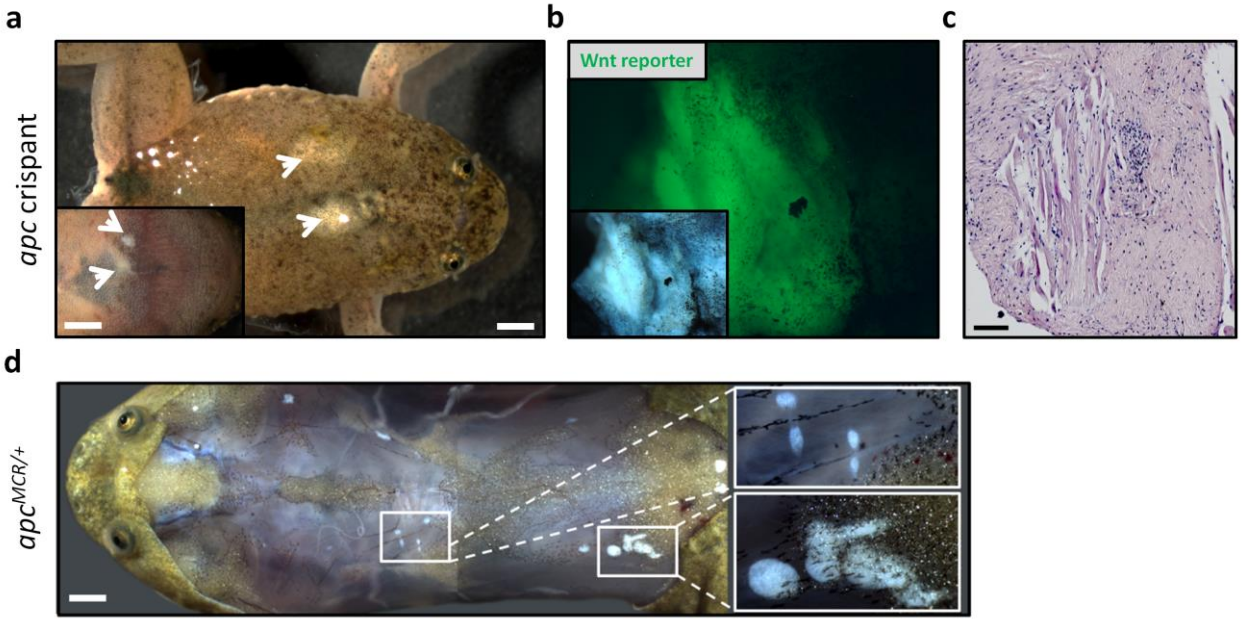

Figure S1: *apc*$^{\Delta 1/+}$ (*apc*$^{MCR/+}$) and *apc* F0 mosaic mutant crispants develop multiple desmoid tumors (DT) reminiscent of the extra-colonic manifestations of familial adenomatous polyposis (FAP). (a) Targeting the MCR of *apc* by the CRISPR/Cas9 technology leads to development of a number of DTs both dorsally and ventrally (inset). **(b)** These DTs exhibit active Wnt signaling as demonstrated here by activation of a Wnt reporter construct[13]. **(c)** Histopathology of these tumors revealed hallmarks of desmoid tumors such as sweeping fascicles of uniform, spindle shaped cells with local invasion into musculature. White scale bars are 0.2 cm and black scale bar is 100 µm. **(d)** An *apc*$^{\Delta 1/+}$ animal (aged 18 months), euthanized and with skin removed, manifesting multiple DTs associated with thoracolumbar fascia, as well as superficial and deep dorsal muscles. Insets represent higher magnifications of clusters of these DTs.

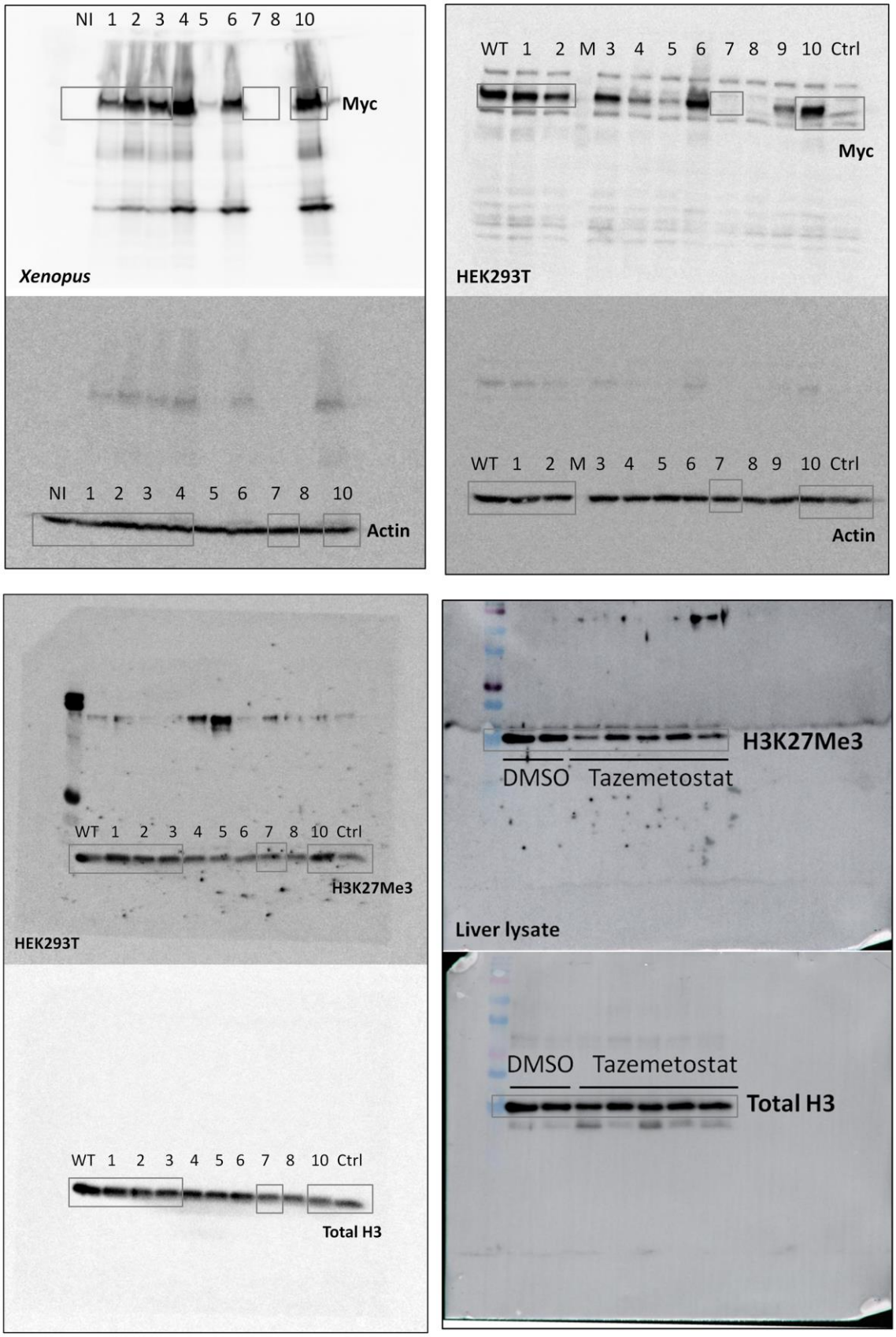
NI 1 2 3 4 5 6 7 8 10
Myc
Xenopus
NI 1 2 3 4 5 6 7 8 10
Actin
WT 1 2 M 3 4 5 6 7 8 9 10 Ctrl
Myc
HEK293T
WT 1 2 M 3 4 5 6 7 8 9 10 Ctrl
Actin
WT 1 2 3 4 5 6 7 8 10 Ctrl
H3K27Me3
HEK293T
WT 1 2 3 4 5 6 7 8 10 Ctrl
Total H3
H3K27Me3
DMSO Tazemetostat
Liver lysate
DMSO Tazemetostat
Total H3

Figure

S2: Uncropped western blots. Following legend was used. Parts of blots used in Figure 2 are demarcated by grey boxes.

(NI) not injected

(1) NM_00101793.2:c.2163_2180del;

(2) NM_001017293.2:c.2165_2182del;

(3) NM_001017293.2:c.2171_2179del;

(4)NM_001017293.2:c.143_178del;

(5) NM_001017293.2:c.127_147del;

(6) NM_001017293.2:c.144_149del;

(7) NM_001017293.2:c.2068_2074del;

(8) NM_001017293.2:c.2068del;

(9) NM_001017293.2:c.2170_2171insAAACAA;

(10) NM_001017293.2:c.2127A>T,

(ctrl) pMAX-GFP

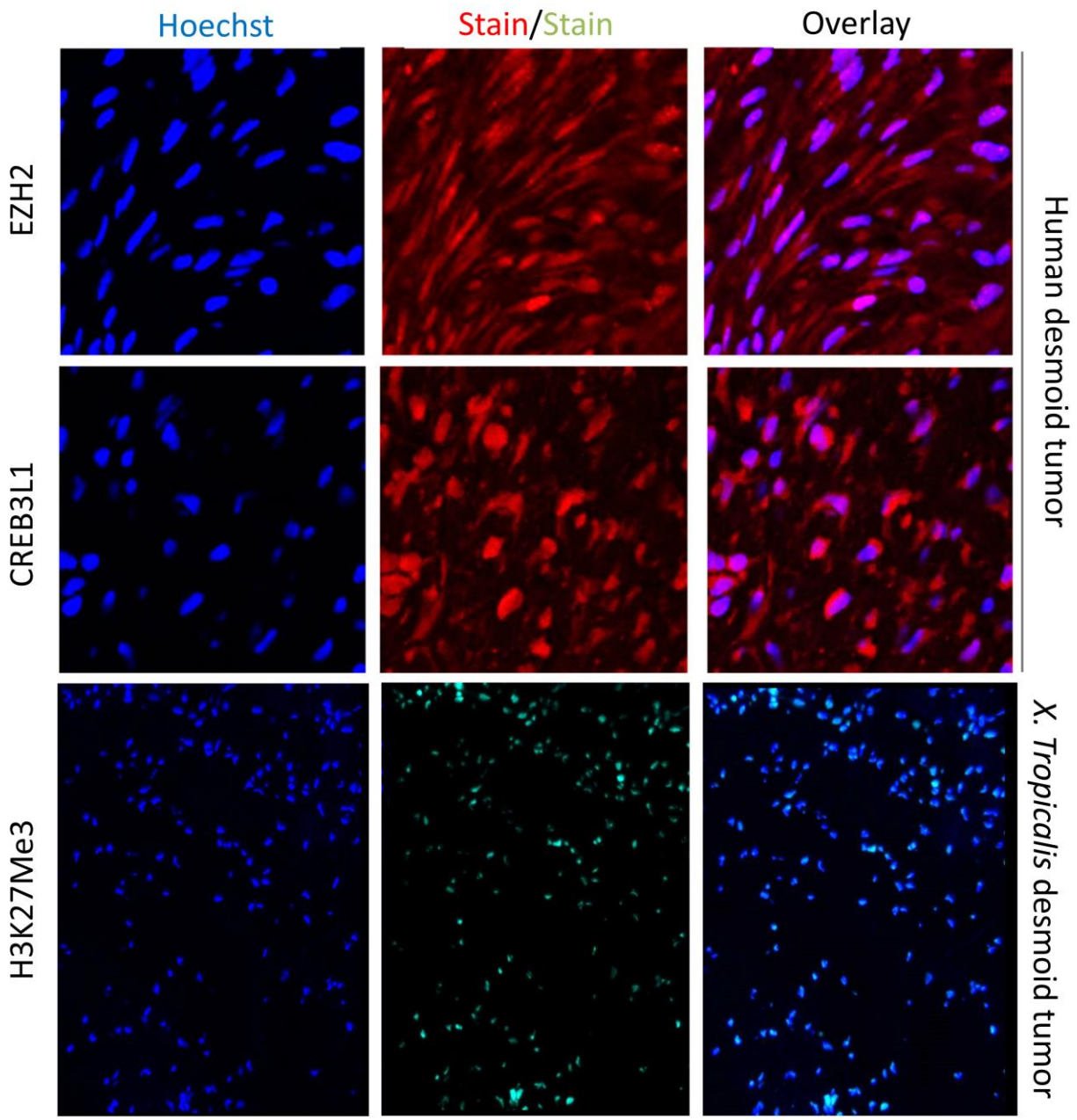

Fig. S3: Immunostaining reveals CREB3L1 and EZH2 expression in human desmoid tumor cells and H3K27me3 immunoreactivity in *X. tropicalis* desmoid tumors.

Table S1: Genotyping by PCR amplification, sequencing (MiSeq) and BATCH-GE analysis. Data table containing quantitative genome editing efficiency assessments.

Table S2: Multiclass differential expression analyses. Results of differential expression analysis and gene set enrichment analysis of the genes upregulated in desmoid tumors compared to other fibrotic lesions

Table S3: Compiling a list of potential genetic dependencies. Table with a schematic overview of putative dependency factors included in the screening and the rational towards their inclusion in the list.

Table S4: CRISPR-NSID tumor sequencing. Data table containing both a synopsis of the dominant variant calls obtained for all genes under scrutiny in the CRISPR-NSID screen and the raw quantitative genome editing assessment with associated frequencies of all variant calls.

Table S5: CRISPR-NSID analysis. Data tables for the analysis of the CRISPR-NSID screening data in order to achieve binomial probabilities.

Table S6: Statistical Analyses. Data tables containing statistical analyses.

Table S7: Sequences of primers used to generate gRNAs, generate PCR amplicons and concentrations of gRNA/Cas9 employed for *Xenopus tropicalis* genome engineering.